On the Dynamics of Chaotic Systems with Multiple Attractors: A Case Study

J. Kengne, A. Nguomkam Negou, D. Tchiotsop, V. Kamdoum Tamba and G.H. Kom

Abstract In this chapter, the dynamics of chaotic systems with multiple coexisting attractors is addressed using the well-known Newton–Leipnik system as prototype. In the parameters space, regions of multistability (where the system exhibits up to four disconnected attractors) are depicted by performing forward and backward bifurcation analysis of the model. Basins of attraction of various coexisting attractors are computed, showing complex basin boundaries. Owing to the fractal structure of basin boundaries, jumps between coexisting attractors are predicted in experiment. A suitable electrical circuit (i.e., analog simulator) is designed and used for the investigations. Results of theoretical analysis are verified by laboratory experimental measurements. In particular, the hysteretic behavior of the model is observed in experiment by monitoring a single control resistor. The approach followed in this chapter shows that by combining both numerical and experimental techniques, one can gain deep insight into the dynamics of chaotic systems exhibiting multiple attractor behavior.

1 Introduction

It is well known that nonlinear dynamical systems can develop various forms of complexity such as bifurcation, chaos, hyperchaos, and intermittency, just to name a few. The occurrence of two or more asymptotically stable equilibrium points or attracting sets (e.g., period-*n* limit cycle, torus, chaotic attractor) as the system parameters are being monitored represents another striking and complex behavior observed in nonlinear systems. In a system developing coexisting attractors, the trajectories selec-

J. Kengne (✉) · A. Nguomkam Negou · D. Tchiotsop · G.H. Kom
Laboratoire d'Automatique et Informatique Appliquée (LAIA), Department of Electrical Engineering, IUT-FV Bandjoun, University of Dschang, Dschang, Cameroon
e-mail: kengnemozart@yahoo.fr

A. Nguomkam Negou · V. Kamdoum Tamba
Laboratory of Electronics and Signal Processing, Department of Physics, University of Dschang, 67, Dschang, Cameroon

K. Kyamakya et al. (eds.), *Recent Advances in Nonlinear Dynamics and Synchronization*, Studies in Systems, Decision and Control 109,
DOI 10.1007/978-3-319-58996-1_2

tively converge to either of the attracting sets depending on the initial state of the system. Correspondingly, the basin of attraction of an attractive set is defined as the set of initial points whose trajectories converge to the given attractor. The boundary separating each basin of attraction can be a smooth boundary or riddled basin with no clear demarcation (i.e., fractal). This striking and interesting phenomenon has been encountered in various nonlinear systems including lasers [1], biological systems [2, 3], chemical reactions [4], Lorenz systems [5], Newton–Leipnik systems [6], and electrical circuits [7–11]. Such a phenomenon is connected primarily to the system symmetry and may be accompanied by some special effects such as symmetry-breaking bifurcation, symmetry-restoring crisis, coexisting bifurcations, and hysteresis [12–15]. In practice, the coexistence of multiple attractors implies that an attractor may suddenly jump to a different attractor, the situation in which coexisting attractors possess a fractal or intermingled basin of attraction being the most intriguing. In this case, due to noise, the observed signal may be the result of random switching of the system trajectory between two or more concurrent coexisting attractors. This chapter deals with the dynamics of the Newton–Leipnik equation considered as a prototypal dynamical system with multiple coexisting attractors. First of all, let us review some interesting works related to the analysis and control of this particular system. The mathematical model of the so-called Newton–Leipnik system was introduced by Newton and Leipnik [6] in 1981. The Euler rigid-body equations were modified with the addition of linear feedback. A system of three quadratic differential equations was obtained that for certain feedback gains develops two strange attractors. The attractor for an orbit was determined by the location of the initial point for that orbit. In [16], Wang and Tian consider the bifurcation analysis and linear control of the Newton–Leipnik system as a prototypal dynamic system with two strange attractors. The static and dynamic bifurcations of the model are studied. Chaos controlling is performed by a linear controller, and numerical simulation of the control is supplied. Further results on the dynamics and bifurcations of the Newton–Leipnik equation were provided by Lofaro [17]. The authors used numerical computations and local stability calculations to suggest that the dynamics of the Newton–Leipnik equations are related to the dynamics and bifurcations of a family of odd symmetric bimodal maps. The article [18] also studies the dynamical behavior of the Newton–Leipnik system and its trajectory-transformation control problem to multiple attractors. A simple linear state feedback controller for the Newton–Leipnik system based on Lyapunov stability theory and application of the inverse optimal control strategy is designed. Chaotic attractors are stabilized asymptotically to unstable equilibria of the systems, so that the transformation of one attractor to another for the trajectory of the Newton–Leipnik system is realized. In [19], it is shown how a chaotic system with more than one strange attractor can be controlled. Issues in controlling multiple (coexisting) strange attractors as stabilizing a desired motion within one attractor as well as taking the system dynamics from one attractor to another are addressed. Realization of these control objectives is demonstrated using as a numerical example the Newton–Leipnik equation. Motivated by the above-mentioned results, this chapter proposes a methodological analysis of the Newton–Leipnik equation considered as a prototypal dynamical system with multiple coexisting attractors. Regions of mul-

tiple attractor behavior (i.e., hysteretic dynamics) are illustrated using bifurcation diagrams computed based on suitable techniques. Furthermore, basins of attraction of various coexisting attractors are also computed to visualize how the various coexisting attractors magnetize the state space. Owing to the fast computation speed of analog computers, we suggest that such an apparatus can be advantageously exploited to investigate nonlinear systems with multiple attractors such as the Newton–Leipnik equation. The rest of the chapter is structured as follows. Section 2 describes the mathematical model of the Newton–Leipnik system. Some basic properties of the model are underlined with practical implications for the occurrence of multiple attractors. In Sect. 3, the bifurcation structures of the system are investigated numerically showing period-doubling and symmetry-recovering crisis phenomena. Regions of the parameters space corresponding to the occurrence of multiple coexisting attractors are depicted. Correspondingly, basins of attraction of various coexisting solutions are computed showing complex basin boundaries. A suitable electrical circuit (i.e., analog computer) that can be exploited for the analysis of the Newton–Leipnik equation is proposed in Sect. 4. Finally, some concluding remarks are presented in Sect. 5.

2 Description and Analysis of the Model

2.1 The Model

The mathematical model of the Newton–Leipnik equation [6] considered in this chapter is expressed by the following set of three coupled first-order nonlinear differential equations:

$$\begin{aligned} \dot{x}_1 &= -ax_1 + x_2 + bx_2x_3, \\ \dot{x}_2 &= -x_1 - ax_2 + 5x_1x_3, \\ \dot{x}_3 &= cx_3 - 5x_1x_2, \end{aligned} \tag{1}$$

where x_1, x_2, and x_3 are the state variables; a, b, and c are three positive real constants. It can be seen that the model possesses three quadratic nonlinearities in which are involved the three state variables (x_1, x_2, and x_3).

The presence of this nonlinearity is responsible for the complex behaviors exhibited by the whole system. Obviously, system (1) is invariant under the transformation $(x_1, x_2, x_3) \Leftrightarrow (-x_1, -x_2, x_3)$. Therefore, if (x_1, x_2, x_3) is a solution of system (1) for a specific set of parameters, then $(-x_1, -x_2, x_3)$ is also a solution for the same parameter set. The fixed point $E_0(0, 0, 0)$ is a trivial symmetric static solution. Also, attractors in state space have to be symmetric by reflection in the x_3-axis; otherwise, they must appear in pairs to restore the exact symmetry of the model equations. This exact symmetry could serve to explain the presence of several coexisting attractors in state space [20, 21]. Furthermore, it represents a good way to check the scheme used for numerical analysis. It is important to note that for typical parameters values $a = 0.4$, $b = 10$, $c = 0.175$, system (1) has five equilibrium points, which are

all unstable [18, 19]. Also, for these parameter values, the system experiences self-excited oscillations [22, 23].

2.2 Dissipation and Existence of Attractors

Preliminary insights related to the existence of attractors in Newton–Leipnik systems can be gained by evaluating the volume contraction rate [20, 21] of the model. Briefly recall that the volume contraction rate of a continuous-time dynamical system described by $\dot{x} = \varphi(x)$, where $x=(x_1, x_2, x_3)^T$ and $\varphi(x)=(\varphi_1(x), \varphi_2(x), \varphi_3(x))^T$, is given by

$$\Lambda = \nabla.\varphi(x) = \frac{\partial \varphi_1}{\partial x_1} + \frac{\partial \varphi_2}{\partial x_2} + \frac{\partial \varphi_3}{\partial x_3}. \tag{2}$$

We note that if Λ is a constant, then the time evolution in phase space is determined by $V(t) = V_0 e^{\lambda(t)}$, where $V_0 = V(t = 0)$. Thus, a negative value of Λ leads to a fast exponential shrinkage (i.e., damped) of the volume in state space; the dynamical system is dissipative and can experience or develop attractors. For $\Lambda = 0$, phase space volume is conserved, and the dynamical system is conservative. If Λ is positive, the volume in phase space expands, and hence there exist only unstable fixed points or cycles or possibly chaotic repellors [20, 21]; in other words, the dynamics diverge as the system evolves (i.e., for $t \to \infty$) if the initial conditions do not coincide exactly with one of the fixed points or stationary states. Referring to the model in (1), it can easily be shown that $\Lambda = c - 2a < 0$ independently of the position $(x_1, x_2, x_3)^T$ in state space; hence system (1) is dissipative, and thus can support attractors.

3 Numerical Study

3.1 Numerical Methods

In order to examine the rich variety of dynamical behaviors that can be observed in a Newton–Leipnik system, we solve numerically system (1) using the classical fourth-order Runge–Kutta integration algorithm. For each set of parameters used in this chapter, the time step is always $\Delta t = 0.005$ and the calculations are carried out using variables and constant parameters in extended mode. For each parameter setting, the system is integrated for a sufficiently long time and the transient is canceled. Two indicators are used to identify the type of scenario giving rise to chaos. The bifurcation diagram represents the first indicator, the second indicator being the graph of the largest Lyapunov exponent (λ_{max}). Concerning the latter case, the dynamics of the system is classified using its Lyapunov exponent, which is computed numerically using the algorithm described by Wolf and collaborators [24]. In

particular, the sign of the largest Lyapunov exponent determines the rate of almost all small perturbations to the system's state, and consequently, the nature of the underlined dynamical attractor. For $\lambda_{max} < 0$, all perturbations vanish, and trajectories starting sufficiently close to each other converge to the same stable equilibrium point in state space; for $\lambda_{max} = 0$, initially close orbits remains close but distinct, corresponding to oscillatory dynamics on a limit cycle or torus; and finally, for $\lambda_{max} > 0$, small perturbations grow exponentially, and the system evolves chaotically within the folded space of a strange attractor.

3.2 Route to Chaos

To investigate the sensitivity of the system with respect to a single control parameter, we fix $a = 0.6$, $b = 5$ and vary c in the range $0.13 \leq c \leq 0.15$. In monitoring the control parameter, it is found that the Newton–Leipnik system under consideration can experience very rich and striking bifurcation scenarios. Sample results showing bifurcation diagrams for varying c and the corresponding spectrum of largest Lyapunov exponent are provided in Fig. 1a and b respectively.

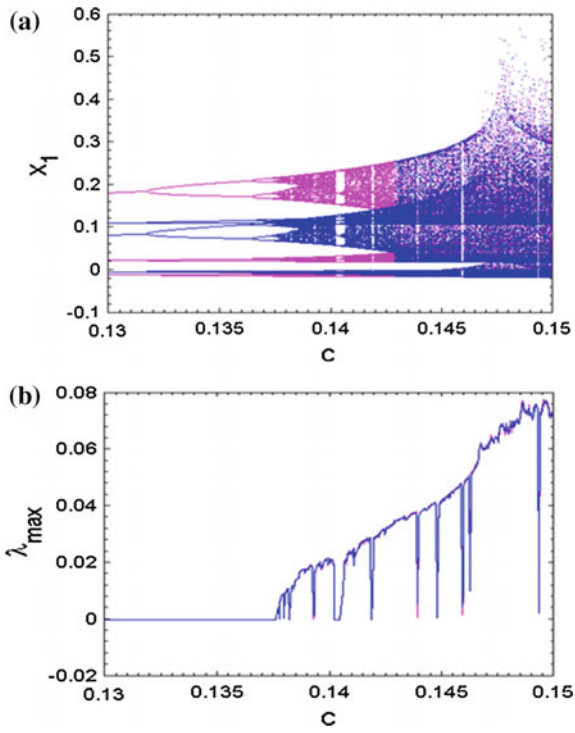

Fig. 1 Bifurcation diagram **a** showing local maxima of the coordinate x_1 versus c and the corresponding graph **b** of largest Lyapunov exponent (λ_{max}) plotted in the range $0.13 \leq c \leq 0.15$. A window of hysteretic dynamics can be noticed for lower values of c. *Magenta* and *blue* diagrams correspond respectively to increasing and decreasing values of c. The positive value of λ_{max} is the signature of chaotic motion: Parameter values $(a, b) = (0.6, 5)$

The bifurcation diagram is obtained by plotting local maxima of the coordinate x_1 in terms of the control parameter, which is increased (or decreased) in tiny steps in the range $0.13 \leq c \leq 0.15$. The final state at each iteration of the control parameter serves as the initial state for the next iteration. In the graph of Fig. 1a, two sets of data corresponding to increasing (blue) and decreasing (magenta) values of c are superimposed. This strategy, known as forward and backward continuation, represents a simple way to localize the window in which the system develops multiple coexisting attractor behaviors (see Sect. 4). In light of Fig. 1a and b, the following bifurcation sequence emerges when the control parameter c is slowly increased. For values of c under the critical value $c_c = 0.11$, the system exhibits periodic oscillations (i.e., period-3 limit cycle). On increasing the control parameter c past this critical value, a stable period-3 limit cycle born from the Hopf bifurcation undergoes a series of period-doubling bifurcations, culminating in a single-band spiraling chaotic attractor. On further increasing c up to $c_{cr1} = 0.1402$, a periodic window suddenly appears in which the system displays a period-8 and then a single-band chaotic attractor. Past the critical value $c_{cr2} = 0.143$, the single-band chaotic attractor suddenly changes to a double-band chaotic attractor following a symmetry-recovering crisis. Also note the presence of many tiny windows of periodic motions sandwiched in the chaotic bands. It can be seen that the bifurcation diagram coincides well with the spectrum of the Lyapunov exponent. With the same parameter settings in Fig. 1, various

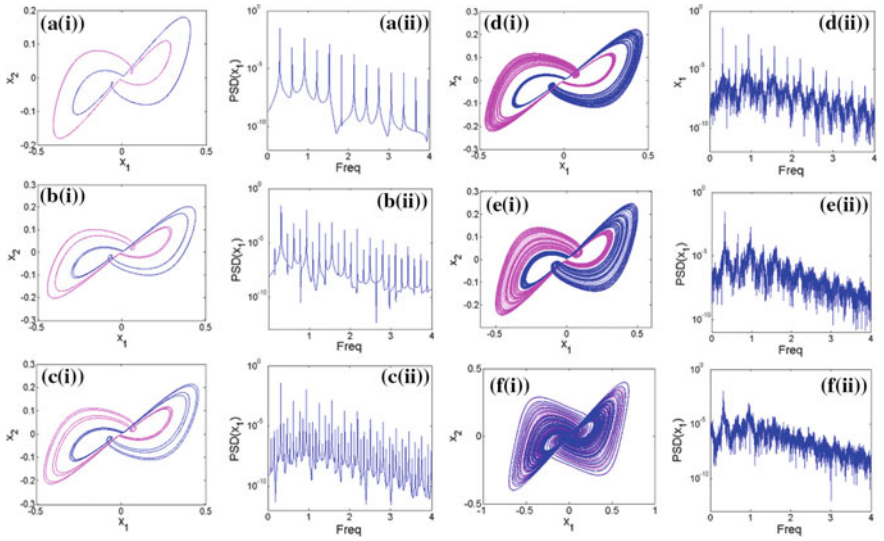

Fig. 2 Two-dimensional views of the attractor projected onto the (x_1, x_2)-plane (*left*) of the system, showing routes to chaos (in terms of the control parameter c) and corresponding power spectra (*right*): **a** period-1 for $c = 0.13$, **b** period-2 for $c = 0.135$, **c** period-4 for $c = 0.1373$, **d** single-band chaos for $c = 0.1388$, **e** single-band chaos for $c = 0.1328$, **f** double-band for $c = 0.145$. The parameters are those of Fig. 2

numerical phase portraits and corresponding frequency spectra were obtained, confirming different bifurcation sequences depicted previously (see Fig. 2).

It should be noted that for periodic motion, all spikes in the power spectrum are harmonically related to the fundamental, whereas a broadband power spectrum is characteristic of a chaotic mode of oscillations. Briefly recall that the periodicity of an attractor is deduced by counting the number of spikes located at the left-hand side of the highest spike of the spectrum (the latter being included).

3.3 Occurrence of Multiple Attractors

To observe the phenomenon of multiple attractors, two prototypes were considered. The first is obtained by setting $(a, b) = (0.6, 5)$. With reference to the bifurcation diagram of Fig. 1, a window of hysteretic dynamics (i.e., multiple stability) can be identified in the range $0.13 \leq c \leq 0.14$ (see Fig. 3).

For values of c within this range, the long-term behavior of the system depends on the initial state, thus leading to the interesting and striking phenomenon of coexisting multiple attractor behaviors. Up to four different attractors can be obtained depending solely on the selection of initial conditions. For $c = 0.142$, four different chaotic attractors are presented in a phase portrait of (Fig. 4) using different initial conditions $(x_1(0), x_2(0), x_3(0)) = (0, \pm 0.1, \pm 0.01)$.

The second approach is obtained using $(a, b) = (0.73, 10)$. We plot the corresponding bifurcation diagram versus the control parameter c, as well as the corresponding graph of the Lyapunov exponent (see Fig. 5a and b).

In the diagram of Fig. 5a, a window of hysteretic dynamics (and thus multistability) can be identified in the range $0.13 \leq c \leq 0.16$. For values of c within this range, the long-term behavior of the system depends on the initial state; hence the system develops the interesting phenomenon of coexisting multiple attractor behaviors. For

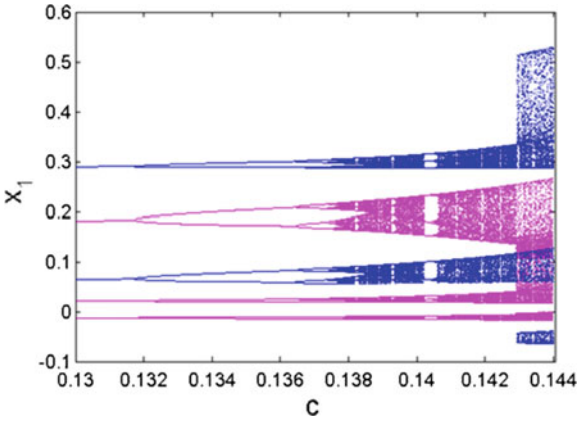

Fig. 3 Enlargement of the bifurcation diagram of Fig. 2 showing the region in which the system exhibits multiple coexisting attractors. This region corresponds to values of c in the range $0.13 \leq c \leq 0.144$. Two sets of data corresponding to increasing (*magenta*) and decreasing (*blue*) values of the control parameter are superimposed

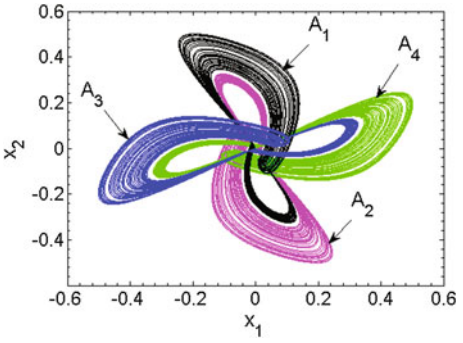

Fig. 4 Coexistence of four different attractors consisting of two pairs of single-band chaotic attractors projected onto the (x_1, x_2)-plane for $(a, b) = (0.6, 5)$ and $c = 0.142$. Initial conditions are $(x_1(0), x_2(0), x_3(0)) = (0, \pm 0.1, \pm 0.01)$

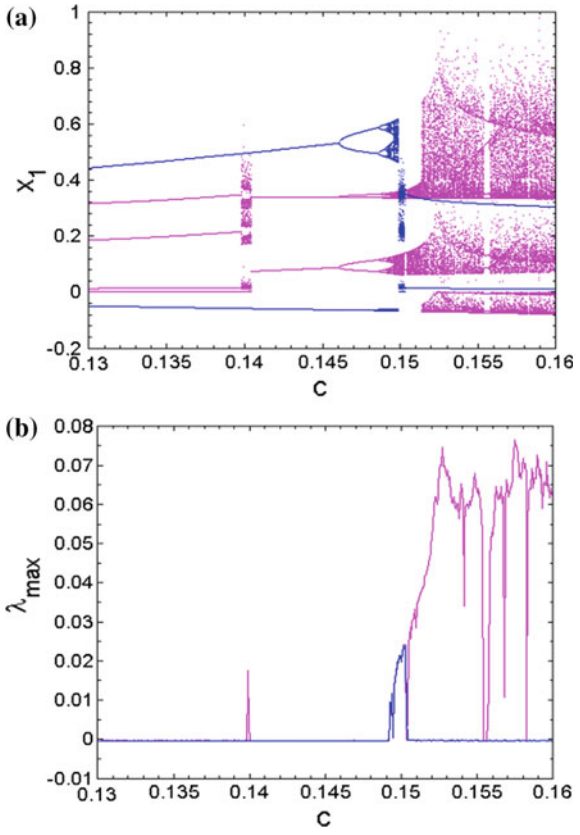

Fig. 5 Bifurcation diagram **a** showing local maxima of the coordinate x_1 versus c and the corresponding graph **b** of the largest Lyapunov exponent λ_{max} plotted in the range $0.13 \leq c \leq 0.16$. A window of hysteretic dynamics can be noticed for some values of c. *Magenta* and *blue* diagrams correspond respectively to increasing and decreasing values of c. The positive value of λ_{max} is the signature of chaotic motion: parameter values $(a, b) = (0.73, 10)$

$c = 0.151$, four different attractors (see Fig. 6d) can be obtained depending only on the selection of initial conditions.

For instance, the pair of period-1 phase portraits and a pair of chaotic attractors of Fig. (6d) can be obtained under the initial conditions $(x_1(0), x_2(0), x_3(0)) = (0, \pm 0.1, \pm 0.01)$. We also see that for $c = 152$, three different attractors (see Fig. 7d) can be obtained depending only on the selection of initial conditions, a pair of

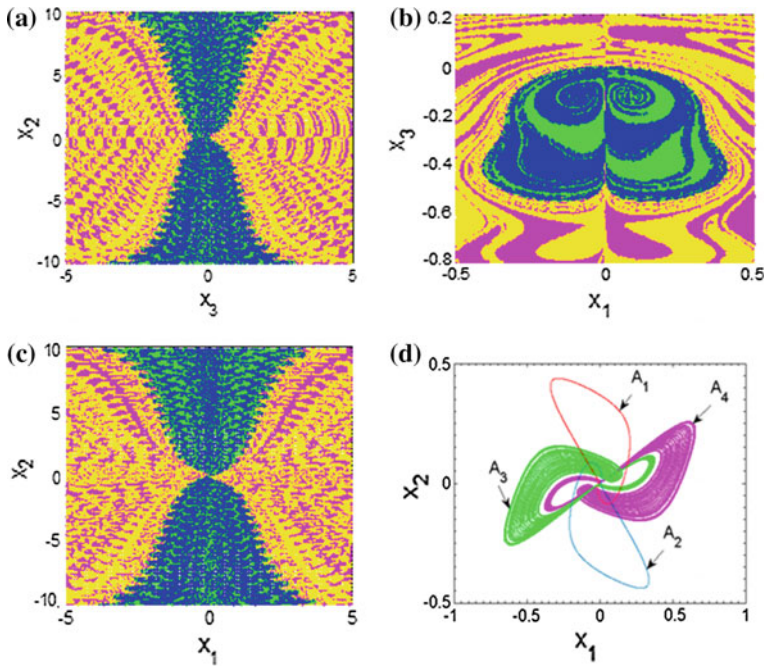

Fig. 6 Cross sections of the basin of attraction **a**, **b**, **c** for $x_1(0) = 0, x_2(0) = 0$, and $x_3(0) = 0$, and $x_3(0) = 0$ respectively and two-dimensional views of four different attractors consisting of a pair of single-band chaotic attractors with a pair of asymmetric period-1 attractors **d** projected onto the (x_1, x_2)-plane for $(a, b) = (0.73, 10)$ and $c = 0.151$. Initial conditions are $(x_1(0), x_2(0), x_3(0)) = (0, \pm 0.1, \pm 0.01)$. *Yellow* and *green* regions correspond to the period-1 pair of attractors, while the *magenta* and *blue* regions are associated with the chaotic solutions obtained for $(a, b, c) = (0.73, 5, 0.151)$

period-1 phases portraits and a double-band chaotic attractor for $(x_1(0), x_2(0), x_3(0)) = (0, \pm 0.1, \pm 0.01)$. Therefore, considering the parameters in Fig. 6d and carrying out a scan of initial conditions (see Fig. 6a–c), we have defined the domain of initial conditions in which each attractor can be found. Figure 6a–c show cross sections of the basin of attraction respectively for $x_1(0) = 0$, $x_2(0) = 0$, and $x_3(0) = 0$ corresponding to the symmetric pair of limit cycles (blue and green) and the pair of chaotic attractors (magenta and yellow). Likewise, considering the parameter setting in Fig. 7d, we have defined the domain of initial conditions in which each attractor can be found.

Figure 7a–c show the structure of the sections of the basin of attraction respectively for $x_1(0) = 0$, $x_2(0) = 0$, and $x_3(0) = 0$. Green and yellow lead to a pair of period-1 limit cycle while magenta regions are associated to the double-band chaotic solution. It should be mentioned that multiple attractor behavior (involving at least

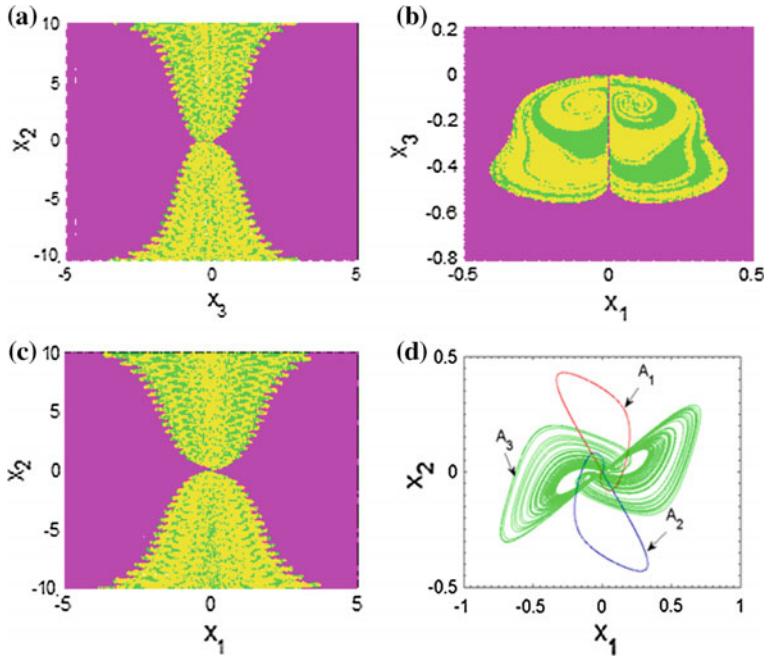

Fig. 7 Cross sections of the basin of attraction **a**, **b**, **c** for $x_1(0) = 0$, $x_2(0) = 0$, and $x_3(0) = 0$ respectively and two-dimensional views of three different attractors consisting of a double-band chaotic attractor with a pair of asymmetric period-1 ones **d** projected onto the (x_1, x_2)-plane. Initial conditions are $(x_1(0), x_2(0), x_3(0)) = (0, \pm 0.1, \pm 0.01)$. *Green* and *yellow* regions correspond to the period-1 pair of attractors, while *magenta* regions are associated with the chaotic solutions obtained for $(a, b, c) = (0.73, 10, 0.152)$

four nonstatic disconnected attractors) is common in various nonlinear systems (see, e.g., Sect. 1). Very recently, Hens and collaborators considered the case of coexistence of infinitely many attractors, also referred to as extreme multistability, in coupled dynamical systems [25]. It is obvious that the occurrence of multiple attractors is an additional source of randomness in chaotic systems that may be exploited for chaos-based secure communication. However, in many other cases, this singular type of behavior is not desirable and it justifies the need for control. Detailed study along this line is beyond the scope of this work; also, interested readers are referred to the review work on control of multistability by Pisarshik and collaborators [26].

4 The Analog Computer Approach

It is well known that even with a very fast computer, scanning the parameter space can turn out to be very time-consuming. Furthermore, there is no rigorous method for selecting the integration step used for the numerical integration as well as the duration of the transient time. These difficulties (as well as many others) faced in performing numerical computation can be overcome by adopting the analog computer approach [27, 28]. One of the merits of the analog computer is the possibility of exploring wide ranges of dynamic behaviors by simply monitoring, for instance, a single control resistor. Nevertheless, the accuracy of the results of analog computation strongly depends on the quality of the electronic components used in the construction of the analog computer. Also, by combining the fast computation speed of an analog simulator and the precision of a digital computer, one can gain deep insight into the dynamics of a given nonlinear process such as the Newton–Leipnik system. Our goal in this section is to design and implement an appropriate analog simulator that can be exploited for the analysis of the model defined in system (1). A circuit diagram of the proposed electronic simulator is provided in Fig. 8. Compared to the

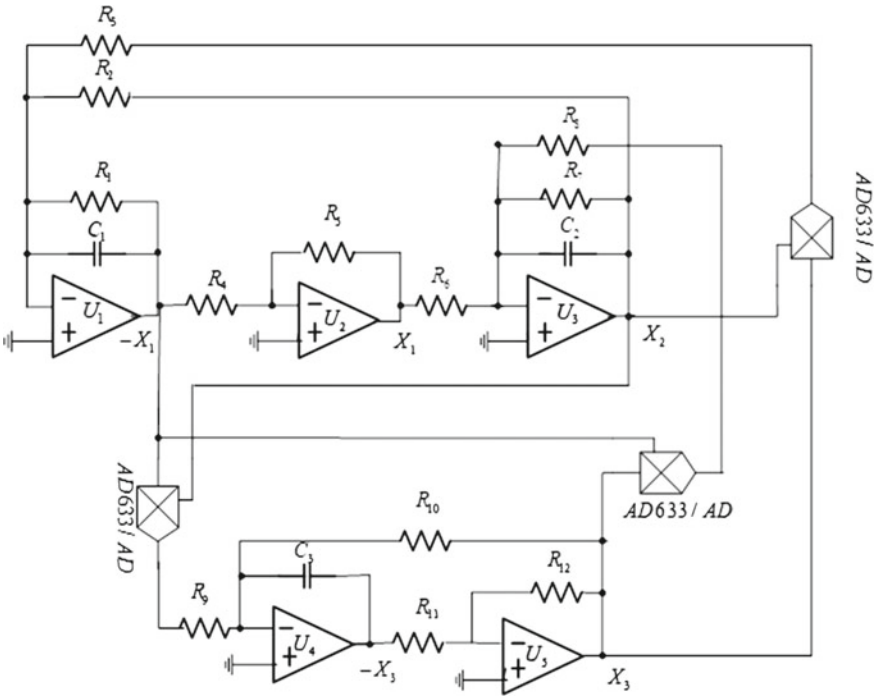

Fig. 8 Electronic circuit realization of a Newton–Leipnik system with three quadratic interactions using $R_1 = R_7 = 16666\Omega$, $R_2 = R_4 = R_5 = R_6 = R_{11} = R_{12} = 10K\Omega$, $R_{10} = 0 - 100K\Omega$, and $C = 10nF$

circuit proposed in [28] (utilizing up to twenty resistors and nine operational (op) amplifiers), the analog simulator shown in Fig. 8 involves a minimum number of electronic components.

The electronic multipliers are the analog devices AD633JN, versions of the AD633 four-quadrant voltage multipliers chips used to implement the nonlinear terms of our model. They operate over a dynamic range of ± 1 V with a typical error less than 1%. They also have a built-in divide-by-ten feature. The signal W at the output depends on the signals at inputs $X_1(+)$, $X_2(-)$, $Y_1(+)$, $Y_2(-)$, and $W = (X_1 - X_2)(Y_1 - Y2)/10 + Z$. The operational amplifiers and associated circuitry implement the basic operations of addition, subtraction, and integration. By adopting an appropriate time scaling, the simulator outputs can be displayed directly on an oscilloscope by connecting the output voltage of X_1 to the X input and the output voltage of X_2 to the Y input. By applying the Kirchhoff current and voltage laws to the circuit in Fig. 8, it can be shown that the voltages X_1, X_2, and X_3 satisfy the set of three coupled first-order nonlinear differential equations

$$\begin{aligned} \frac{dX_1}{dt} &= -\frac{X_1}{R_1C_1} + \frac{X_2}{R_2C_1} + \frac{X_2X_3}{10R_3C_1}, \\ \frac{dX_2}{dt} &= -\frac{X_2}{R_7C_2} - \frac{X_1}{R_6C_2} + \frac{X_1X_3}{10R_8C_2}, \\ \frac{dX_3}{dt} &= \frac{X_3}{R_{10}C_3} - \frac{X_1X_2}{10R_9C_3}. \end{aligned} \tag{3}$$

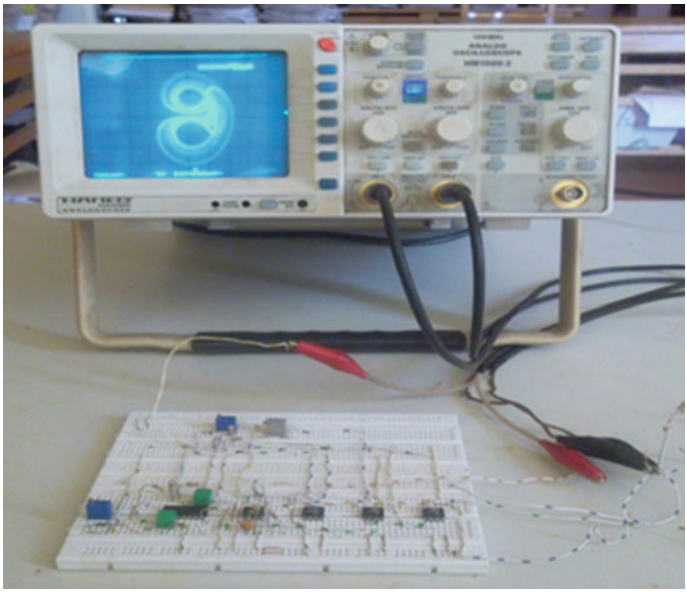

Fig. 9 The experimental Newton–Leipnik simulator in operation

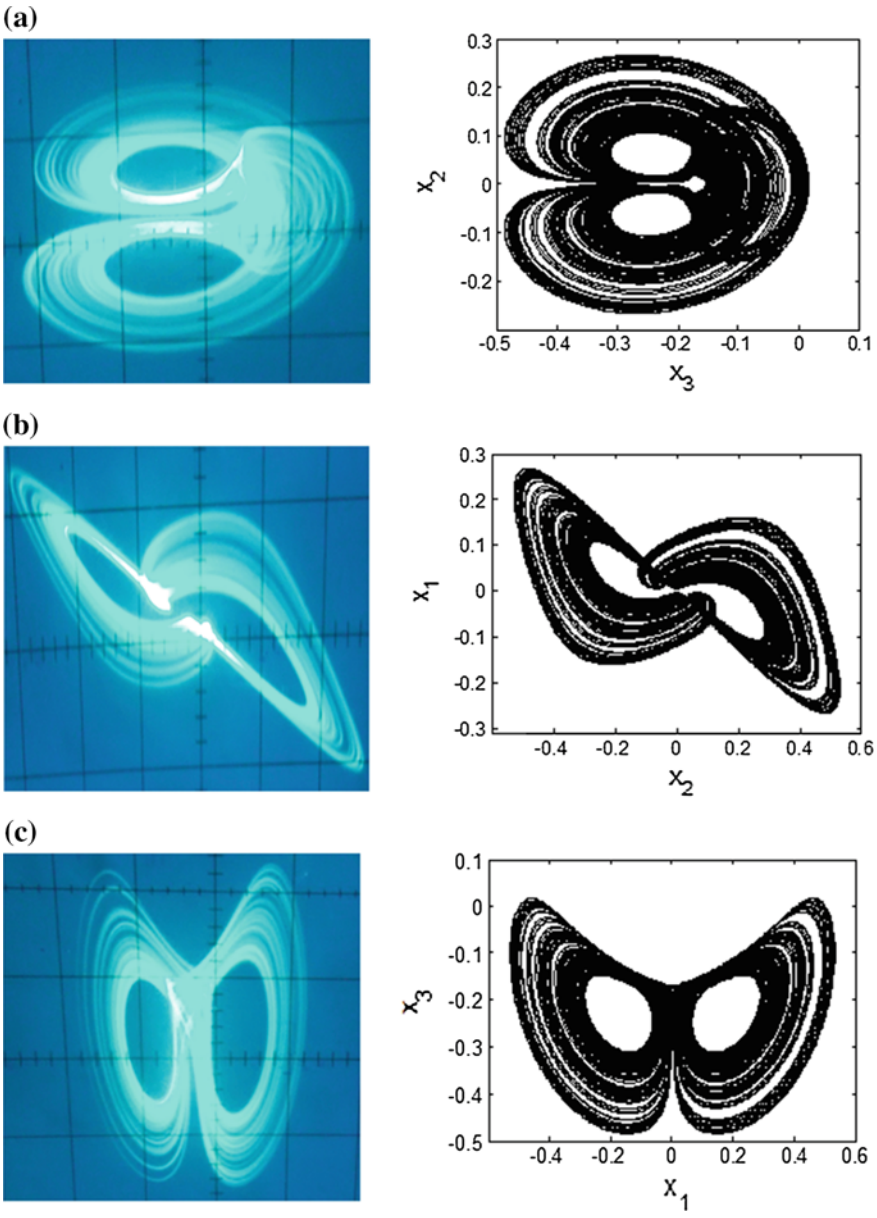

Fig. 10 Experimental phase portraits (*left*) obtained from the circuit using a dual trace oscilloscope in XY mode; the corresponding numerical phase portraits are shown on the *right*, obtained by a direct integration of the system (1) with $(a, b, c) = (0.6, 5, 0.145)$: **a** projection onto the (X_3, X_2)-plane, **b** projection onto the (X_1, X_2)-plane, and **c** projection onto (X_1, X_3)-plane. The scales are $X = 1V/div$ and $Y = 0.5V/div$ for all pictures

With a time unit of 10^4, the parameters of system (1) are expressed in terms of the values of capacitors and resistors as follows (provided that the critical relationships $10^4 R_2 C_1 = 1, 10^4 R_6 C_2 = 1, 5.10^5 R_8 C_2 = 1, 5.10^5 R_9 C_3 = 1$ are satisfied):

$$a = \frac{10^{-4}}{R_1 C_1}, b = \frac{10^{-4}}{R_3 C_1}, c = \frac{10^{-4}}{R_{10} C_3}. \tag{4}$$

We briefly recall that the time scaling process offers to analog devices (operational amplifiers and analog multipliers) the possibility of operating under their bandwidth. Furthermore, time scaling offers the possibility of simulating the behavior of the system at any given frequency by expressing the real time variable τ versus the analog computation time variable $t (t = 10^{-n}\tau)$, allowing the simulation frequency to be less than the real frequency by a factor of order 10^{+n}. In the latter expression, the positive integer depends on the values of resistors and capacitors used in the analog simulator. A photograph of the experimental analog simulator in operation is shown in Fig. 9, while a comparison between numerical and experimental phase portraits is provided in Fig. 10.

From the graphs in Fig. 10, it clearly appears that the dynamics of the Newton–Leipnik system is well reproduced by the analog simulator.

5 Concluding Remarks

This chapter has focused on a methodological analysis of the Newton–Leipnik system considered as a prototypal dynamical system with multiple attractors. Regions of multiple attractors in the parameter space were depicted using bifurcation diagrams based on appropriate techniques (e.g., forward and backward bifurcation diagrams). Furthermore, basins of attraction of various competing attractors were computed, showing nontrivial basin boundaries, thus suggesting possible jumps between different coexisting attractors in experiment. Moreover, one piece of interesting information that can be gained from basins of attraction is the chance of the appearance of attractors in a real system. A suitable electrical circuit (i.e., analog simulator) was designed that was shown to reproduce the Newton–Leipnik attractor. Combined with numerical techniques, the proposed analog computer may be particularly useful for exploring the parameter space in view of tracking further regions of multiple attractors in the Newton–Leipnik model. We stress that the approach followed in this chapter may be exploited advantageously in the investigation of other nonlinear dynamical systems exhibiting multiple attractors.

References

1. Masoller, C.: Coexistence of attractors in a laser diode with optical feedback from a large external cavity. Phys. Rev. A **50**, 2569–2578 (1994)
2. Cushing, J.M., Henson, S.M.: Blackburn: multiple mixed attractors in a competition model. J. Biolog. Dyn. **1**, 347–362 (2007)
3. Upadhyay, R.K.: Multiple attractors and crisis route to chaos in a model of food-chain. Chaos, Solitons Fractals **16**, 737–747 (2003)
4. Massoudi, A., Mahjani, M.G., Jafarian, M.: Multiple attractors in Koper-Gaspard model of electrochemical. J Electroanal. Chem. **647**, 74–86 (2010)
5. Li, C., Sprott, J.C: Coexisting hidden attractors in a 4-D simplified Lorenz system. Int. J. Bifurc. Chaos **24**, 1450034 (2014)
6. Leipnik, R.B., Newton, T.B.: Double strange attractors in rigid body motion with linear feedback control. Phys. Lett. A **86**, 63–87 (1981)
7. Vaithianathan, V., Veijun, J.: Coexistence of four different attractors in a fundamental power system model. IEEE Trans. Cir. Syst. **I46**, 405–409 (1999)
8. Kengne, J.: Coexistence of chaos with hyperchaos, period-3 doubling bifurcation, and transient chaos in the hyperchaotic oscillator with gyrators. Int. J. Bifurc. Chaos **25**(4), 1550052 (2015)
9. Pivka, L., Wu, C.W., Huang, A.: Chua's oscillator: a compendium of chaotic phenomena. J.Frankl. Inst. **331B**(6), 705–741 (1994)
10. Kuznetsov, A.P., Kuznetsov, S.P., Mosekilde, E., Stankevich, N.V.: Co-existing hidden attractors in a radio-physical oscillator. J. Phys. A Math. Theor. **48**, 125101 (2015)
11. Kengne, J., Njitacke, Z.T., Fotin, H.B.: Dynamical analysis of a simple autonomous jerk system with multiple attractors. Nonlinear Dyn. **48**, 751–765 (2016)
12. Li, C., Hu, W., Sprott, J.C., Wang, X.: Multistability in symmetric chaotic systems. Eur. Phys. J. Spec. Top. **224**, 1493–1506 (2015)
13. Letellier, C., Gilmore, R.: Symmetry groups for 3D dynamical systems. J. Phys. A. Math. Theor. **40**, 5597–5620 (2007)
14. Rosalie, M., Letellier, C.: Systematic template extraction from chaotic attractors: I. Genus-one attractors with inversion symmetry. J. Phys. A Math. Theor. **46**, 375101 (2013)
15. Rosalie, M., Letellier, C.: Systematic template extraction from chaotic attractors: II. Genus-one attractors with unimodal folding mechanisms. J. Phys. A Math. Theor. **48**, 235100 (2015)
16. Xuedi, W., Lixin, T.: Bifurcation analysis and linear control of the Newton-Leipnik system. Chaos, Solitons Fractals **27**, 31–38 (2006)
17. Lofaro, T.: A model of the dynamics of the Newton-Leipnik attractor. Int. J. Bifurc. Chaos **7**(12), 2723–2733 (1997)
18. Wang, X., Gao, Y.: The inverse optimal control of chaotic system with multiple attractors. Mod. Phys. Lett. B **21**, 1199–2007 (2007)
19. Hendrik, R.: Controlling chaotic systems with multiple strange attractors. Phys. Lett. A **300**, 182–188 (2002)
20. Strogatz S.H.: Nonlinear Dynamics and Chaos. Addison-Wesley, Reading
21. Nayfeh, A.H., Balachandran, B.: Applied Nonlinear Dynamics: Analytical, Computational and Experimental Methods. Wiley, New York
22. Leonov, G.A., Kuznetsov, N.V.: Hidden attractors in dynamical systems. From hidden oscillations in Hilbert-Kolmogorov, Aizerman, and Kalman problems to hidden chaotic attractor in Chua circuits. Int. J. Bifurc. Chaos **23**, 1793–6551 (2013)
23. Leonov, G.A., Kuznetsov, N.V., Mokaev, T.N.: Homoclinic orbits, and self-excited and hidden attractors in a Lorenz-like system describing convective fluid motion. Eur. Phys. J. Spec. Top. **224**, 1421–1458 (2015)
24. Wolf, A., Swift, J.B., Swinney, H.L., Wastano, J.A.: Determining Lyapunov exponents from time series. Physica D **16**, 285–317 (1985)
25. Pisarchik, A.N., Feudel, U.: Control of multistability. Phys. Rep. **540**(4), 167–218 (2014)
26. Hens, C., Dana, S.K., Feudel, U.: Extreme multistability: attractors manipulation and robustness. Chaos **25**, 053112 (2015)

27. Chedjou, J.C., Fotsin, H.B., Woafo P., Domngang, S.: Analog simulation of the dynamics of a van der Pol oscillator coupled to a Duffing oscillator. IEEE Trans. Circuits Syst. I: Fundam. Theory Appl. **48**, 748–756 (2001)
28. Zhao, R., Song, Y.: Circuit realization of Newton-Leipnik chaotic system via EWB. Chinese control and decision conference, Yantai, Shandong, pp. 5111–5114 (2008)

http://www.springer.com/978-3-319-58995-4

Recent Advances in Nonlinear Dynamics and Synchronization

With Selected Applications in Electrical Engineering, Neurocomputing, and Transportation

Kyamakya, K.; Mathis, W.; Stoop, R.; Chedjou, J.C.; Li, Z. (Eds.)

2018, XII, 367 p. 137 illus., 69 illus. in color., Hardcover
ISBN: 978-3-319-58995-4